Broad-Band Microstrip-to-CPW Transition via Frequency-Dependent Electromagnetic Coupling

Lei Zhu, *Senior Member, IEEE,* and Wolfgang Menzel, *Fellow, IEEE*

***Abstract*—An improved broad-band microstrip-to-coplanar-waveguide (CPW) transition is developed on a basis of the frequency-dependence characteristic of an electromagnetic surface-to-surface coupling. A self-calibrated method of moments is extended to model this unbounded two-port discontinuity with the two dissimilar microstrip/CPW feeding lines. Numerical results are provided to demonstrate its frequency response of transmission under varied strip/slot dimensions and further exhibit its attractive ultra-broad-band transmission with low radiation loss. Next, the back-to-back transition circuits with the two different lengths are fabricated and measured to deembed in experiment the S-parameters of two single-transition structures. Predicted and measured results show good agreement with the return loss less than −10 dB over the frequency of 3.2–11.2 GHz.**

***Index Terms*—Broad-band, electromagnetic (EM) coupling, experimental deembedding, method of moments (MoM), microstrip-to-coplanar-waveguide (CPW) transition, short–open calibration (SOC).**

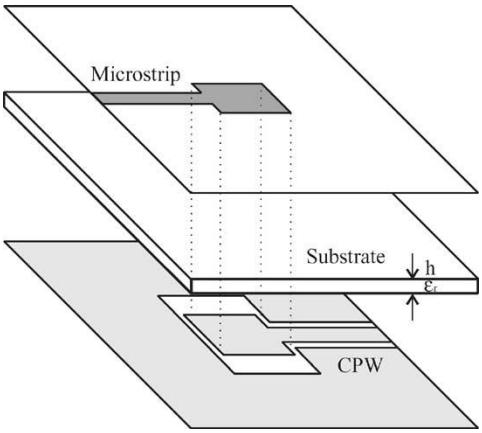

Fig. 1. Layout of the proposed microstrip-to-CPW transition via EM coupling.

I. Introduction

BROAD-BAND microstrip-to-coplanar-waveguide (CPW) transitions or interconnects without bonding wires [1]–[9] have been arousing an endless interest in the exploitation of hybrid and/or multilayered microwave integrated circuits due to several exclusive features of microstrip and CPW lines. Stemming from the idea of a CPW-to-CPW transition [10], a so-called surface-to-surface transition structure [1]–[3] was successfully developed via electromagnetic (EM) coupling of the microstrip and CPW at different layers. Intuitively speaking, this transition operates on a basis of the quarter-wavelength asymmetric parallel-coupled line theorem, e.g., [11]. The broad-band transmission behavior with low return loss was realized by widening the two slots in the CPW and the central strip conductor in the microstrip [1] or installing an additional microstrip matching circuit [3]. According to the principle of the microstrip-to-slotline transition, an alternative microstrip-to-CPW transition was recently developed using two pairs of open-circuited microstrip and short-circuited slotline stubs with radial shape [4]. Moreover, a few transition structures were presented in [7]–[9] to realize the wave transmission between the microstrip and CPW with a finite ground width.

In this paper, an improved broad-band microstrip-to-CPW transition is proposed using the frequency-dependent behavior of the surface-to-surface coupling [1]–[3] with extended coupled-strip conductors [12]. Due to enhanced capacitive coupling in series between microstrip and CPW strip conductors, the overall transmission passband can be expanded with two rejection zeros [13]. Following [14] and [15], this two-port transition structure with the two dissimilar microstrip and CPW feeders is characterized by implementing the short–open calibration (SOC) procedure in the full-wave method of moments (MoM). Thus, electrical performance of such a transition is numerically deembedded via two sets of SOC standards. Next, two types of back-to-back transition circuits are fabricated and measured for experimental deembedding of their actual behaviors over a wide frequency range. Both predicted and measured results show excellent broad-band characteristic with the bandwidth of 91%–111% for the return loss below −10 dB.

II. Geometry Description and Modeling Technique

Fig. 1 depicts the geometrical layout of the proposed two-port microstrip-to-CPW transition driven with the microstrip and CPW feeders. Herein, the two coupled-strip surfaces in conjunction with the lower CPW and upper microstrip are largely widened while the twin-slot width in the CPW is properly incremented, making up a frequency-dependent parallel-coupled microstrip/CPW section with tight coupling. Following the early research in [12] and [13], this coupled-strip structure can be perceived as an enhanced equivalent series-capacitive element at low frequency and a parallel-coupled transmission line with a tightly distributed coupling degree as frequency increases. Thus, this transition is expected to hold the broad-band

Manuscript received November 18, 2003; revised January 19, 2004.

L. Zhu is with the School of Electrical and Electronic Engineering, Nanyang Technological University, Singapore 639798 (e-mail: ezhul@ntu.edu.sg).

W. Menzel is with the Department of Microwave Techniques, University of Ulm, D-89069 Ulm, Germany (e-mail: menzel@mwt.e-technik.uni-ulm.de).

Digital Object Identifier 10.1109/TMTT.2004.827034

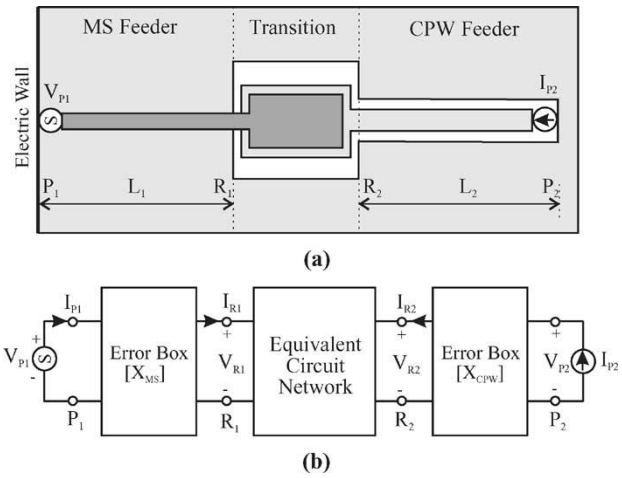

Fig. 2. Physical model and equivalent-circuit topology for full-wave MoM modeling of the two-port microstrip-to-CPW transition. (a) MoM model. (b) Equivalent topology.

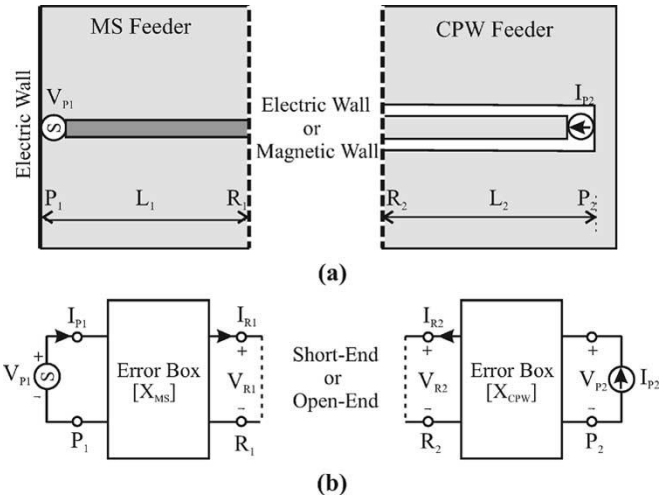

Fig. 3. Physical model and equivalent-circuit network of two pairs of microstrip and CPW SOC calibration standards. (a) MoM model. (b) Equivalent network.

transmission behavior with the high upper-end frequency, in which the coupled-strip length is approximately equal to the half-wavelength, as achieved in [12], [13], and [16].

First of all, a self-calibrated MoM technique [14], [15] is extended to model such a two-port transition structure. Fig. 2(a) shows the schematic of this transition in the source-type MoM platform. To do it, an impressed voltage source V_{P1} backed by an electric wall is introduced at the terminal of the microstrip feeder, while an impressed current source I_{P2} is assumed at the center of a transverse slot for the CPW feeder. Herein, the two source ports P_1 and P_2 should be selected far away from the transition module so that all the higher order modes generated by impressed sources disappear at the two references R_1 and R_2. As detailed in [14] and [15], a set of coupled mixed-field integral equations can be established by enforcing the boundary conditions over the upper strip conductor and lower slot area, and they can be derived in the spectral domain with three distinct parts, i.e., microstrip feeder, transition, and CPW feeder, through the electric and magnetic dyadic Green's functions [17], [18].

According to the Galerkin's technique, the unknown electric- and magnetic-current densities are expressed in terms of superposition of a set of piecewise-sinusoidal and pulse basis functions, while the similar-waveform weighting functions are selected with the same number as above. As such, the coupled integral equations can be converted into the source-type matrix equation for numerical implementation, resulting in the solution of the total electric-current density over the upper strip conductor and equivalent magnetic-current density over the lower slot. Thus, the current (I_{P1}) and voltage (V_{P2}) can be derived as a function of the impressed port voltage (V_{P1}) and current (I_{P2}), respectively, thereby deducing the two-port network h-parameters [19] at the two ports P_1 and P_2.

Fig. 2(b) describes the equivalent-circuit topology with the three distinct circuit blocks in the cascaded connection in conjunction with the overall transition under modeling. The two different error boxes $[X_{MS}]$ and $[X_{\rm CPW}]$ represent the electrical behavior of the microstrip and CPW feeders driven by the two nonideal impressed sources, respectively. Of course, they take into account all the parasitic effects of the port discontinuities caused by the approximate excitation mechanism at the two ports. The central network indicates the core two-port transition block to be characterized. In order to deembed the central block using the SOC technique, the two sets of paired short- and open-end elements [14] need to be defined in the consistent MoM for both microstrip and CPW feeders.

As illustrated in Fig. 3(a), two such sets of perfect microstrip and CPW SOC calibration standards can be constructed by terminating the microstrip and CPW feeders at the two references R_1 and R_2 with vertical electric and magnetic walls. In the MoM, these walls can be realizing by adding an imaging electric- and magnetic-current density introduced at the symmetrical location with respect to R_1 and R_2, respectively, for the microstrip and CPW feeders. By executing the MoM simulation of these two sets of short and open circuits, the two-port network parameters of each error box can be numerically derived in a consistent manner to the MoM modeling of the transition itself. Fig. 3(b) shows the equivalent two-port networks with the short or open end at R_1 and R_2, respectively, in which the network parameters of $[X_{MS}]$ or $[X_{\rm CPW}]$ can be obtained relying on the MoM-calculated currents (I_{R1} and I_{P1}) [14] or voltages (V_{R2} and V_{P2}) [15]. Thus, the core transition network can be deembedded or extracted by calibrating out two such MoM-characterized error boxes on a basis of the equivalent cascaded topology in Fig. 2(b).

III. Predicted Results

With the use of this MoM–SOC technique, the two-port scattering- or S-matrix parameters of a variety of microstrip-to-CPW transition structures can be derived. Fig. 4(a) depicts the layout of a simple structure: transition (A), in

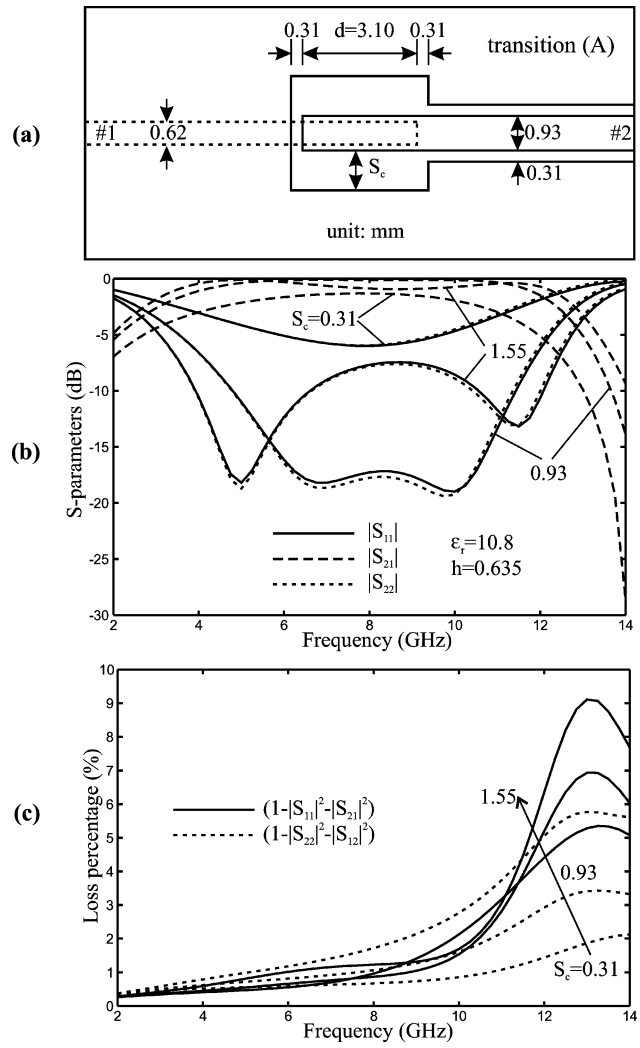

Fig. 4. Geometry and simulated frequency response of the microstrip-to-CPW transition (A). (a) Layout. (b) S-parameters. (c) Loss percentage.

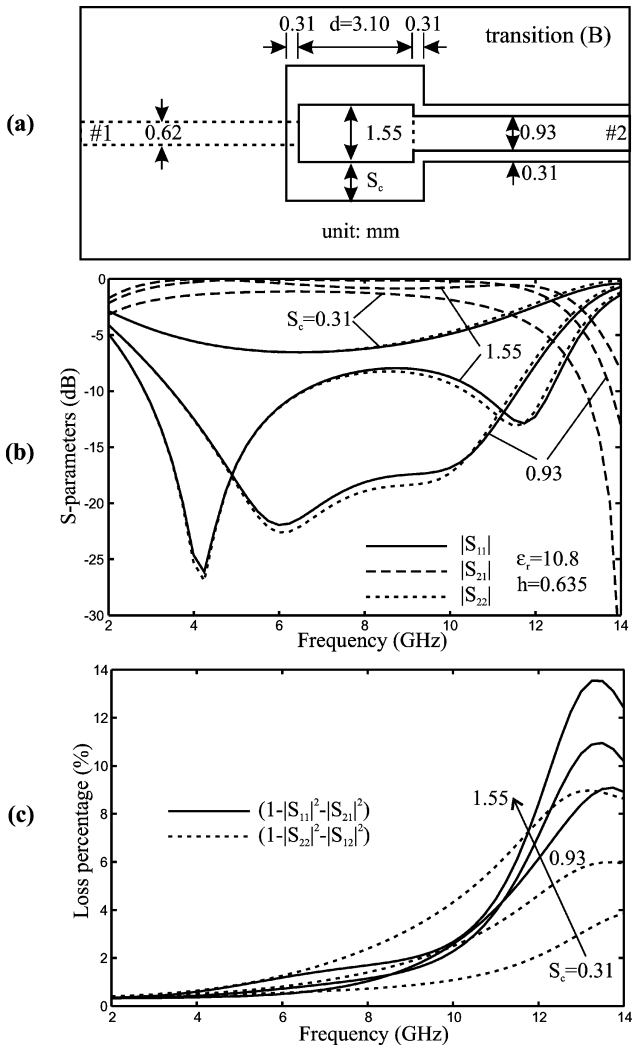

Fig. 5. Geometry and simulated frequency response of the microstrip-to-CPW transition (B). (a) Layout. (b) S-parameters. (c) Loss percentage.

which the twin slots with the width of S_c are simultaneously widened, while the strip conductors of both microstrip and CPW sections are kept unchanged in width. Intuitively, the EM coupling between the lower and upper strip conductors should become tight as S_c is enlarged, thus raising the equivalent series capacitive coupling between them, as denoted in [12]. Fig. 4(b) plots the three sets of simulated S- parameters under the selected slot widths of $S_c = 0.31, 0.93$, and 1.55 mm. Firstly, the unfavorable frequency response with S_{21} less than -1.2 dB can be seen for $S_c = 0.31$ mm due to its insufficient strip-to-strip coupling.

As S_c increases to 0.93 and 1.55 mm, S_{11} falls down to constitute a broad passband with two minimum values or rejection zeros [16] and then it goes up in the frequency range between these two zeros. Such a variation in its passband can be physically attributed to the two maximum peaks of the normalized J-inverter susceptance with reference to characteristic admittances of the two different feeders [16]. Fig. 4(c) depicts the MoM-calculated frequency-related loss percentage, illustrating that the radiation loss is really very small, especially in the frequency range below 12 GHz. Moreover, due to its geometrical asymmetry, its two reflection coefficients are found slightly unequal, as in Fig. 4(b), i.e., $S_{11} \neq S_{22}$, thus, bringing out the observable difference between the two sets of loss factors with regarding to the wave incident to the CPW and microstrip feeders, respectively, as in Fig. 4(c).

Next, the coupled-strip conductors at the upper and lower interfaces are simultaneously widened to the identical width of 1.55 mm so as to construct the transition (B), as indicated in Fig. 5(a), toward further expanding the transmission passband. Fig. 5(b) depicts the simulated frequency response under three different S_c. It is observed here that the lower end of such a passband is moved to the low frequency, while its higher end counterpart is almost unchanged under the half-wavelength limitation of the coupled-strip section, as interpreted in [12] and [16]. As such, transition (B) can achieve the more enhanced passband superior to transition (A). On the other hand, its radiation loss seems to be raised to some extent, as in Fig. 5(c), but is still kept negligibly small, especially at frequencies below 10 GHz.

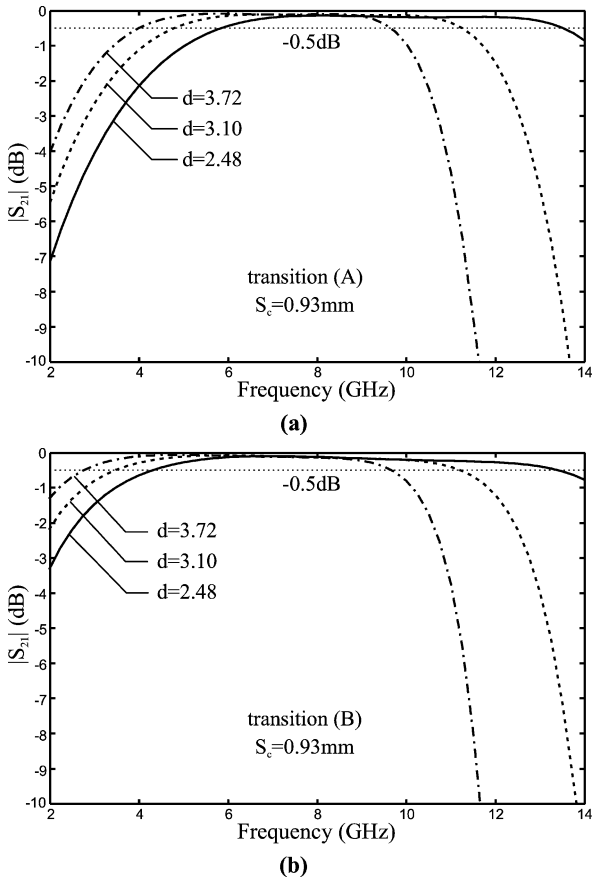

Fig. 6. Frequency-dependent insertion losses of the two transitions versus coupled-strip length (d). (a) Transition (A). (b) Transition (B).

Furthermore, the peak radiation loss for both transitions is observed to happen around 13 GHz, in which the whole CPW slot, surrounded by the coupled-strip conductors, makes up an equivalent full-wavelength slot loop resonator or radiator fed by microstrip and CPW at its two sides.

To further investigate the bandwidth characteristics of these transitions with resorting to other geometrical dimensions, Fig. 6(a) and (b) illustrates the frequency-dependent insertion losses ($|S_{21}|$) of transitions (A) and (B), as described in Figs. 3(a) and 4(a), versus different coupled-strip length (d). It can be observed that as d is enlarged, the wide passband gradually moves down and $|S_{21}|$ is consistently kept above -0.2 dB over the passband regardless of different length (d). By looking at Fig. 6(a) and (b) together, we can again see here that transition (B) always achieves the broader bandwidth than transition (A) under the identical d of choice. It is referred to the fact that the tightened series capacitive coupling in transition (B) with the widened coupled-strip width causes the shift down of the lower end of the passband, while its upper end is almost unchanged.

IV. Experimental Validation

Considering the asymmetrical geometry of the single transition, the back-to-back transition circuit block is constructed by cascading the two single transitions through a uniform CPW section for experimental study. Fig. 7(a) depicts the schematic of such a back-to-back transition, and its relevant equivalent circuit network is illustrated in Fig. 7(b). In the experiment, the two back-to-back transition circuits with the central connecting CPW of different lengths l_1 and l_2 are fabricated and their relevant S-matrix can be measured with the two independent S-parameters for each back-to-back block, i.e., $S_{11}^{\mathrm{I}} = S_{22}^{\mathrm{I}}$ and $S_{12}^{\mathrm{I}} = S_{21}^{\mathrm{I}}$ for $l_1 = 10.00$ mm and $S_{11}^{\mathrm{II}} = S_{22}^{\mathrm{II}}$ and $S_{12}^{\mathrm{II}} = S_{21}^{\mathrm{II}}$ for $l_2 = 14.13$ mm. Thus, the S-matrix of the single microstrip-to-CPW transition can be explicitly deembedded on a basis of the three-cascaded blocks in Fig. 7(b) and their three elements s_{11}, $s_{21} = s_{12}$, and s_{22} can be expressed with the above-measured two sets of S-parameters and the propagation constant (γ) of a uniform CPW via relation between the S-matrix and chain matrix [19]

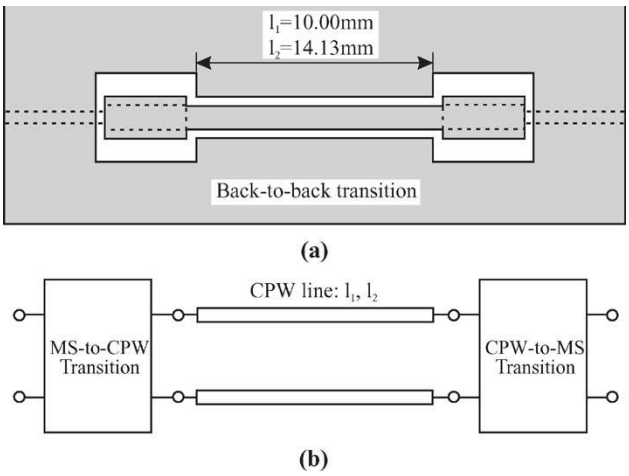

Fig. 7. Geometry and equivalent topology of a generalized back-to-back microstrip-to-CPW transition for experimental deembedding. (a) Geometry. (b) Equivalent cascaded topology.

$$s_{11} = \frac{S_{11}^{\mathrm{I}} S_{21}^{\mathrm{II}} e^{-\gamma l_2} - S_{11}^{\mathrm{II}} S_{21}^{\mathrm{I}} e^{-\gamma l_1}}{S_{21}^{\mathrm{II}} e^{-\gamma l_2} - S_{21}^{\mathrm{I}} e^{-\gamma l_1}} \tag{1}$$

$$s_{22} = \frac{S_{11}^{\mathrm{II}} - S_{11}^{\mathrm{I}}}{S_{21}^{\mathrm{II}} e^{-\gamma l_2} - S_{21}^{\mathrm{I}} e^{-\gamma l_1}} \tag{2}$$

$$s_{21}^2 = \frac{2 S_{21}^{\mathrm{II}} S_{21}^{\mathrm{I}} \sinh\left[\gamma(l_1 - l_2)\right]}{S_{21}^{\mathrm{II}} e^{-\gamma l_2} - S_{21}^{\mathrm{I}} e^{-\gamma l_1}}. \tag{3}$$

Fig. 8 depicts the experimental deembedded S-parameters of the two types of single microstrip-to-CPW transitions against those calculated from the MoM–SOC technique. The measured results are found in excellent agreement with our prediction over the frequency range of 2.0–14.0 GHz, giving an experimental validation on the broad-band transmission behaviors of the proposed transition structure. As seen in Fig. 8(a) and (b), the transmission passband of transitions (A) and (B) cover the frequency ranges of 7.2 and 8.0 GHz, respectively, under the return loss below -10 dB. In other words, their bandwidth in experiment achieves 91% and 111% with reference to their different central frequency of 7.9 and 7.2 GHz, thereby exhibiting that the latter is really superior to the former in bandwidth. As expected

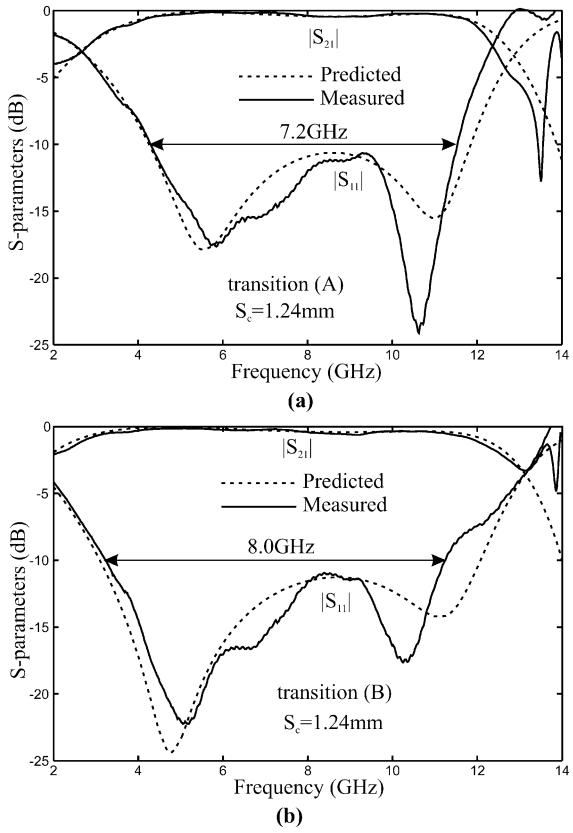

Fig. 8. Experimental deembedded S-parameters of the two single microstrip-to-CPW transitions as compared with those obtained in theory. (a) Transition (A). (b) Transition (B).

early, it is attributed to the fact that the low end of the passband is reduced to a great extent with the widened coupled-strip conductors.

However, measured $|S_{21}|$ is observed to have a sudden dip near 14 GHz, while the calculated one decreases monotonously with frequency. In fact, at the upper end of the frequency range of interest, the difference between the two central lengths, i.e., $l_1 - l_2 = 4.13$ mm, of the two back-to-back transitions comes close to the half-wavelength ($\lambda/2$). Similar to any other calibration method in the RF experiment, such as the thru-reflection line (TRL), in which the length of the line standard must be shorter than $\lambda/2$, as pointed out in [20], the accuracy of such a deembedding technique is no longer as good as at low frequencies, and this resonance-caused dip cannot be properly removed in theory.

V. Conclusions

In this paper, an improved broad-band microstrip-to-CPW transition has been proposed using the tight-coupling and frequency-dependence characteristics of the parallel-coupled strip surfaces in a microstrip and CPW. By widening the twin slots in the CPW and further expanding the two strip conductors in width, the ultra-broad transmission behavior can be realized. With the use of our self-calibrated MoM algorithm, two types of transition structures have been characterized to demonstrate their attractive features such as broad passband and low radiation loss. Furthermore, the back-to-back transition circuit blocks with the two different connecting CPW lengths at the center are fabricated and measured. The experimental deembedded frequency response of two single microstrip-to-CPW transitions provides an excellent validation on the proposed structure over a wide frequency range.

References

[1] J. J. Burke and R. W. Jackson, "Surface-to-surface transition via electromagnetic coupling of microstrip and coplanar waveguide," *IEEE Trans. Microwave Theory Tech.*, vol. 37, pp. 519–525, Mar. 1989.

[2] H. Jin, R. Vahldieck, J. Huang, and P. Russer, "Rigorous analysis of mixed transmission line interconnects using the frequency-domain TLM method," *IEEE Trans. Microwave Theory Tech.*, vol. 41, pp. 2248–2255, Dec. 1993.

[3] G. Strauss and W. S. Menzel, "Millimeter-wave monolithic integrated circuit interconnects using electromagnetic field coupling," *IEEE Trans. Comp., Packag., Manufact. Technol. B*, vol. 19, pp. 278–282, May 1996.

[4] T. H. Lin, "Via-free broad-band microstrip to CPW transition," *Electron. Lett.*, vol. 37, no. 15, pp. 960–962, July 2001.

[5] T. J. Ellis, J.-P. Rashkin, L. P. B. Katehi, and G. M. Rebeiz, "A wideband CPW-to-microstrip transition for millimeter-wave packaging," in *IEEE MTT-S Int. Microwave Symp. Dig.*, 1999, pp. 629–632.

[6] A. M. E. Safwat, K. A. Zaki, W. Johnson, and C. H. Lee, "Novel design for coplanar waveguide to microstrip transition," in *IEEE MTT-S Int. Microwave Symp. Dig.*, 2001, pp. 607–610.

[7] G. Strauss, P. Ehret, and W. Menzel, "On-wafer measurement of microstrip-based MIMIC's without via holes," in *IEEE MTT-S Int. Microwave Symp. Dig.*, 1996, pp. 1399–1402.

[8] G. P. Gauthier, L. P. Katehi, and G. M. Rebeiz, "W-band finite ground coplanar waveguide (FGCPW) to microstrip line transition," in *IEEE MTT-S Int. Microwave Symp. Dig.*, 1996, pp. 107–109.

[9] A. M. E. Safwat, K. A. Zaki, W. Johnson, and C. H. Lee, "Novel design for coplanar waveguide to microstrip transition," in *IEEE MTT-S Int. Microwave Symp. Dig.*, 2001, pp. 607–610.

[10] R. W. Jackson and D. W. Matolak, "Surface-to-surface transition via electromagnetic coupling of coplanar waveguide," *IEEE Trans. Microwave Theory Tech.*, vol. MTT-35, pp. 1027–1032, Nov. 1987.

[11] V. K. Tripathi, "Asymmetric coupled transmission lines in an inhomogeneous medium," *IEEE Trans. Microwave Theory Tech.*, vol. MTT-23, pp. 734–739, Sept. 1975.

[12] L. Zhu and K. Wu, "Ultra-broad-band vertical transition for multilayer integrated circuits," *IEEE Microwave Guided Wave Lett.*, vol. 9, pp. 453–455, Nov. 1999.

[13] W. Menzel, L. Zhu, K. Wu, and F. Bögelsack, "On the design of novel compact broad-band planar filters," *IEEE Trans. Microwave Theory Tech.*, vol. 51, pp. 364–370, Feb. 2003.

[14] L. Zhu and K. Wu, "Unified equivalent circuit model of planar discontinuities suitable for field theory-based CAD and optimization of M(H)MICs," *IEEE Trans. Microwave Theory Tech.*, vol. 47, pp. 1589–1602, Sept. 1999.

[15] L. Zhu, "Realistic equivalent circuit model of coplanar waveguide open circuit: Lossy shunt resonator network," *IEEE Microwave Wireless Comp. Lett.*, vol. 12, pp. 175–177, May 2002.

[16] L. Zhu, W. Menzel, K. Wu, and F. Boegelsack, "Theoretical characterization and experimental verification of a novel compact broadband microstrip bandpass filter," in *Proc. Asia–Pacific Microwave Conf.*, Nov. 2001, pp. 625–628.

[17] P. Bernardi and R. Cicchetti, "Dyadic Green's functions for conductor-backed layered structures excited by arbitrary tridimensional sources," *IEEE Trans. Microwave Theory Tech.*, vol. 42, pp. 1474–1483, Aug. 1994.

[18] S. G. Pan and I. Wolff, "Scalarization of dyadic spectral Green's functions and network formalism for three dimensional full-wave analysis of planar lines and antennas," *IEEE Trans. Microwave Theory Tech.*, vol. 42, pp. 2118–2127, Nov. 1994.

[19] D. A. Frickey, "Conversions between S, Z, Y, h, $ABCD$, and T parameters which are valid for complex source and load impedances," *IEEE Trans. Microwave Theory Tech.*, vol. 42, pp. 205–211, Feb. 1994.

[20] "Agilent network analysis applying the 8510 TRL calibration for non-coaxial measurements," Agilent Technol., Palo Alto, CA, Product Note 8150-8A, 2000.

Lei Zhu (S'91–M'93–SM'00) was born in Wuxi, Jiangsu Province, China, in June 1963. He received the B.Eng. and M.Eng. degrees in radio engineering from the Nanjing Institute of Technology (now Southeast University), Nanjing, China, in 1985 and 1988, respectively, and the Ph.D. Eng. degree in electronic engineering from the University of Electro-Communications, Tokyo, Japan, in 1993.

From 1993 to 1996, he was a Research Engineer with Matsushita-Kotobuki Electronics Industries, Ltd., Tokyo, Japan. From 1996 to 2000, he was a Research Fellow with the École Polytechnique de Montréal, University of Montréal, Montréal, QC, Canada. Since July 2000, he has been an Associate Professor with the School of Electrical and Electronic Engineering, Nanyang Technological University, Singapore. His current research interests include the study of planar integrated dual-mode filters, ultra-broad bandpass filters, broad-band interconnects, planar periodic structures, planar antenna elements/arrays, uniplanar CPW/coplanar stripline (CPS) circuits, as well as full-wave MoM modeling of planar integrated circuits and antennas, numerical deembedding or parameter-extraction techniques, field-theory computer-aided design (CAD) synthesis, and optimization design procedures. He is currently an Associate Editor for the *IEICE Transactions on Electronics*.

Dr. Zhu is currently an Editorial Board member for the IEEE TRANSACTIONS ON MICROWAVE THEORY AND TECHNIQUES. He was the recipient of the Japanese Government (Monbusho) Graduate Fellowship (1989–1993), the First-Order Achievement Award in Science and Technology from the National Education Committee in China (1993), the Silver Award of Excellent Invention from the Matsushita-Kotobuki Electronics Industries Ltd., Japan (1996), and the Asia–Pacific Microwave Prize Award presented at the 1997 Asia–Pacific Microwave Conference, Hong Kong.

Wolfgang Menzel (M'89–SM'90–F'01) received the Dipl.-Ing. degree in electrical engineering from the Technical University of Aachen, Aachen, Germany, in 1974, and the Dr.-Ing. degree from the University of Duisburg, Duisburg, Germany, in 1977.

From 1979 to 1989, he was with the Millimeter-Wave Department, AEG, Ulm, Germany [now the European Aerospace, Defense, and Space Systems, (EADS)]. From 1980 to 1985, he was Head of the Laboratory for Integrated Millimeter-Wave Circuits. From 1985 to 1989, he was Head of the entire Millimeter-Wave Department. During that time, his areas of interest included planar integrated circuits (mainly on the basis of fine-line techniques), planar antennas, and systems in the millimeter-wave frequency range. In 1989, he became a Full Professor with the University of Ulm, Ulm, Germany. His current areas of interest are multilayer planar circuits, waveguide filters and components, antennas, millimeter-wave and microwave interconnects and packaging, and millimeter-wave application and system aspects.

Dr. Menzel is currently an associate editor for the IEEE TRANSACTIONS ON MICROWAVE THEORY AND TECHNIQUES. From 1997 to 1999, he was a Distinguished Microwave Lecturer for Microwave/Millimeter Wave Packaging. From 1997 to 2001, he chaired the German IEEE Microwave Theory and Techniques (MTT)/Antennas and Propagation (AP) Chapter. He was the recipient of the 2002 European Microwave Prize.